Dalton Transactions

PAPER

View Article Online
View Journal | View Issue

Cite this: *Dalton Trans.*, 2015, **44**, 1790

Versatile properties of $CaGd_2ZnO_5:Eu^{3+}$ nanophosphor: its compatibility for lighting and optical display applications

G. Seeta Rama Raju, E. Pavitra, Goli Nagaraju and Jae Su Yu*

Received 15th October 2014,
Accepted 10th November 2014

DOI: 10.1039/c4dt03181d

www.rsc.org/dalton

Red color-emitting $CaGd_2ZnO_5:Eu^{3+}$ (CGZO:Eu^{3+}) nanophosphors were synthesized by a facile sol–gel process. The structural and luminescent properties of these phosphors were investigated as a function of annealing temperature and Eu^{3+} ion concentration. The orthorhombic phase was confirmed at different annealing temperatures, showing an irregular morphology within the nanoscale range. Photoluminescence (PL) excitation spectra of CGZO:Eu^{3+} showed host absorption band (HAB), charge transfer band (CTB), and intense f–f transitions of Eu^{3+} in the violet and blue wavelength regions. The CTB intensity increased and the HAB intensity decreased with increasing annealing temperature or Eu^{3+} ion concentration. The CGZO:Eu^{3+} exhibited a strong absorption in the blue region as compared to the CTB and had a superior property compared to available commercial phosphors. This feature facilitates the fabrication of high color rendering index white light-emitting diodes for display systems. In PL spectra, an intense red emission was observed due to the hypersensitive $^5D_0 \rightarrow {}^7F_2$ transition with good asymmetry ratio and chromaticity coordinates. Optimized annealing temperature and concentration of Eu^{3+} ions were observed for CGZO host lattice based on the 466 nm excitation wavelength. The cathodoluminescent properties were also similar to the PL results.

Introduction

Inorganic oxide phosphors are in increasing demand due to their potential applications in different fields such as biomedical applications, plasma display panels, light-emitting diodes (LEDs), cathode ray tubes, fingerprint detection, sensors, *etc.*[1–10] With the emerging global energy crisis, solid-state lighting-based white LEDs (WLEDs) have made tremendous progress over the past decade due to their good luminous efficiency, low power consumption, reliability, and environmental friendliness.[6,11] Among different kinds of WLEDs, phosphor-converted WLEDs (pc-WLEDs) are extensively used and are very important because they significantly reduce global power requirements and the use of fossil fuels.[12] These pc-WLEDs are fabricated by coating yellow phosphor on the surface of InGaN/GaN blue LED chips, but they have poor color rendering index (CRI) caused by color deficiency in the red region.[12] Currently, red phosphors used for GaN-based LEDs are nitridosilicate and sulfide phosphors. Nitrodosilicate phosphor exhibits a very broad and deep red emission that does not have a high luminous efficacy of radiation,[11] and sulfide phosphor shows a chemical instability and low efficiency.[13] The commercially available red color-emitting oxide phosphor of $Y_2O_3:Eu^{3+}$ has stable physical and chemical properties, but it has weak absorption in the blue region. Therefore, the availability of red phosphors under blue light excitation continues to be a challenge. In this context, our efforts have been focused on the development of a physically and chemically stable red color-emitting oxide phosphor with strong absorption in the blue wavelength region.

In recent times, different kinds of oxide host materials, such as silicates,[14] phosphates,[15] molybdates,[3] tungstates,[16] titanates,[17] zirconates,[18] *etc.*, have been explored for obtaining different kinds of emissions in the visible region. Among the oxide phosphors, binary[1] and ternary[17] compounds have been studied extensively. However, nowadays, oxide-based quaternary compounds are emerging as attention grabbing phosphors. For instance, $A_4RE_6(XO_4)_6O_2$ [14] and ARE_2MO_5 [19] (A = alkaline earth elements, RE = rare earth elements, X = Si or P, and M = Co, Ni, Cu, Zn, Pd or Pt) compounds are established as having the desired luminescent properties for the fabrication of efficient optical systems. Xu *et al.*[20] reported a novel $CaGd_2ZnO_5$ (CGZO) host lattice with GdO_7, CaO_{11}, and ZnO_5 polyhedral units based on the ARE_2MO_5 structure, Mishra *et al.*[21] studied the limited luminescent properties of CGZO:Eu^{3+}, but no

Department of Electronics and Radio Engineering, Kyung Hee University, 1 Seocheon-dong, Giheung-gu, Yongin-si, Gyeonggi-do 446-701, Republic of Korea. E-mail: jsyu@khu.ac.kr; Fax: +82-31-206-2820; Tel: +82-31-201-3820

other reports have been found on this host lattice. The main advantage of CGZO host lattice is the strong blue absorption when doped with Eu^{3+} ions as compared to the commercial Y_2O_3:Eu^{3+} phosphors.

In this paper, we reported the phase stability and annealing temperature effect on the transmittance and luminescent properties of CGZO:Eu^{3+} nanophosphors obtained *via* a sol–gel process for the first time. The structural, morphological, and optical properties were evaluated by X-ray diffraction (XRD) patterns, scanning electron microscope (SEM) images, and UV-visible transmittance spectra, respectively. The photoluminescent excitation (PLE), photoluminescence (PL) emission, and low-voltage electron beam excitation-based cathodoluminescent (CL) properties were investigated. To examine the emission richness, the synthesized CGZO:Eu^{3+} phosphors were compared with the commercially available Y_2O_3:Eu^{3+} and YAG:Ce^{3+} phosphors under similar measurement conditions.

Experimental

Eu^{3+} ion-activated CGZO nanophosphors were prepared by means of a facile sol–gel method. Stoichiometric amounts of high purity (Sigma-Aldrich) grade calcium nitrate tertrahydrate [$Ca(NO_3)_2{\cdot}4H_2O$], gadolinium nitrate hexahydrate [$Gd(NO_3)_3{\cdot}6H_2O$], europium nitrate pentahydrate [$Eu(NO_3)_3{\cdot}5H_2O$], zinc nitrate hexahydrate [$Zn(NO_3)_2{\cdot}6H_2O$] and citric acid [$HOC(COOH)(CH_2COOH)_2$] were used. First, a solution was prepared by dissolving 1 M of $Ca(NO_3)_2{\cdot}4H_2O$, $2(1-x)$ M of $Gd(NO_3)_3{\cdot}6H_2O$, $2x$ M of $Eu(NO_3)_3{\cdot}5H_2O$, and 1 M $Zn(NO_3)_2{\cdot}6H_2O$ in 200 ml de-ionized water. After few minutes of stirring, 8 M of citric acid (1 : 2 ratio of metal ions and citric acid) was added to the metal ions solution and stirring was continued for a minimum of 2 h without heating for the formation of a homogeneous solution. In order to get homogeneous heating of the solution in the beaker, the beaker was closed with a cap and then the solution was heated on a hot plate at 80 °C (solution temperature) with continued magnetic stirring for 1 h. After opening the cap, the solution was evaporated gradually and a yellowish wet gel was formed. The obtained wet gel was dried at 120 °C in an oven for 12 h, and thus a porous solid matrix called xerogel was formed due to liquid expulsion from the pores (syneresis) and capillary pressure-related substantial matrix shrinkage. This xerogel was decomposed to give black-colored flakes with extremely fine particle size on further heating at 400 °C for 3 h. The resulting sample was further annealed at different temperatures ranging from 800 to 1250 °C for 5 h.

XRD patterns of the CGZO:Eu^{3+} phosphor powders after annealing at different temperatures were recorded using a Mac Science (M18XHF-SRA) X-ray powder diffractometer with Cu Kα radiation (1.5406 Å). The morphology of the samples was examined by using a field emission SEM (Zeiss, LEO SUPRA 55), fitted with an energy dispersive X-ray spectrometer. The transmittance spectra of CGZO:Eu^{3+} phosphors as a function of annealing temperature were measured using a CARY 300 Bio (Varian) UV-visible spectrophotometer. The room-temperature PL and PLE spectra were measured using a Photon Technology International (PTI, USA) fluorimeter with a Xe arc lamp of 60 W power and the lifetime was measured with a phosphorimeter attachment to the main system with a Xe flash lamp (25 W power). The quantum yield measurement as a function of excitation wavelength was carried out using a fluorescence spectrophotometer equipped with integrating sphere (Hamamatsu Photonics C9920-02). The CL properties were measured by a Gatan (UK) MonoCL3 system attached to a scanning electron microscope (Hitachi S-4300 SE).

Results and discussion

In order to examine the structural properties, initially, 5 mol% Eu^{3+} ion-doped CGZO (CGZO:5Eu^{3+}) phosphors were synthesized at different annealing temperatures. Fig. 1(a) shows the XRD patterns of CGZO:5Eu^{3+} phosphors obtained at different annealing temperatures ranging from 800 to 1250 °C. Very recently, Xu *et al.*[20] reported the novel CGZO host lattice, and so its JCPDS card is not available. As the annealing temperature increased from 800 to 1200 °C, the XRD patterns were in good agreement with those of Xu *et al.*, and confirmed the orthorhombic phase of typical CGZO diffraction peaks with the space group of *Pbnm*. However, on increasing the annealing temperature over 1200 °C, the Gd_2O_3 monoclinic phase was dominant along with the presence of ZnO peaks. Therefore, the optimum annealing temperature for the CGZO:5Eu^{3+} phosphor was found to be 1200 °C. Furthermore, using the intense diffraction peaks, the crystallite sizes were calculated by the Scherrer equation of $D_{hkl} = k\lambda/\beta\cos\theta$, where D is the average crystallite size, λ is the X-ray wavelength (1.5406 Å), k is the shape factor (0.9), β is the full width at half maximum, and θ is the diffraction angle of an observed peak. The average crystallite sizes were 42.2, 51.05, 66.75, 80, and 86.7 nm at 800, 900, 1000, 1100, and 1200 °C. Fig. 1(b) shows the low- and high-resolution SEM images of the CGZO:5Eu^{3+} phosphors, which show an irregular morphology with nanometer sized particles. Fig. 1(c) shows the energy dispersive X-ray (EDX) spectrum. This confirmed the presence of Ca, Gd, Eu, Zn, and O elements.

Fig. 2 shows the UV-visible transmittance spectra of the CGZO:5Eu^{3+} phosphors as a function of annealing temperature. It was observed that the transmittance decreased when increasing the annealing temperature up to 1100 °C, indicating the decreased band gap of CGZO:5Eu^{3+}. This lowering of the band gap with increasing annealing temperature was clearly observed between 200 and 260 nm of the transmittance spectra. Here, the absorption peaks were narrowed and absorption edge shifted towards the higher energy region. However, due to the stabilized orthorhombic phase, improved crystallinity, and increased band gap by widening the absorption edge with the doping of Eu^{3+} ions in the CGZO host lattice, the transmittance increased at 1200 °C. For further clarification, the transmittance spectra of CGZO:5Eu^{3+} and pure CGZO

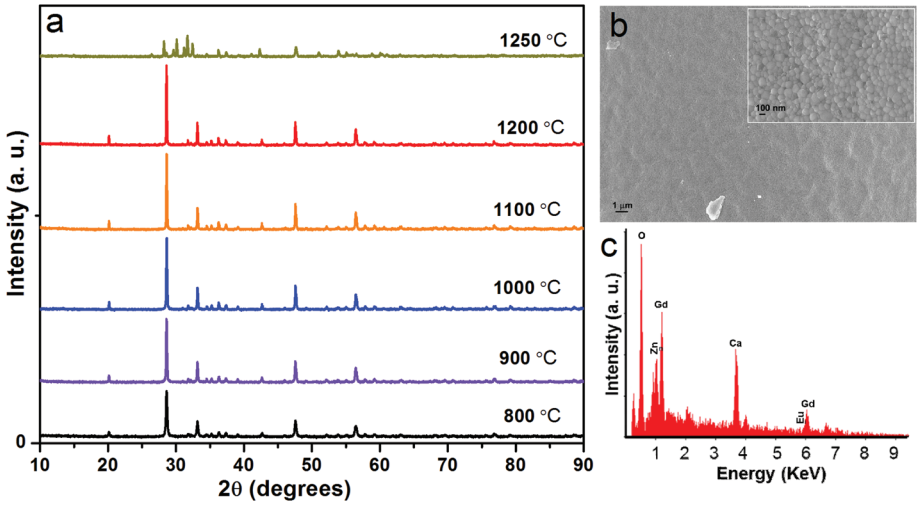

Fig. 1 (a) XRD patterns of the CGZO:5Eu^{3+} phosphors obtained at different annealing temperatures, (b) SEM image (inset shows a magnified SEM image), and (c) EDX pattern of the CGZO:5Eu^{3+} phosphor annealed at 1200 °C.

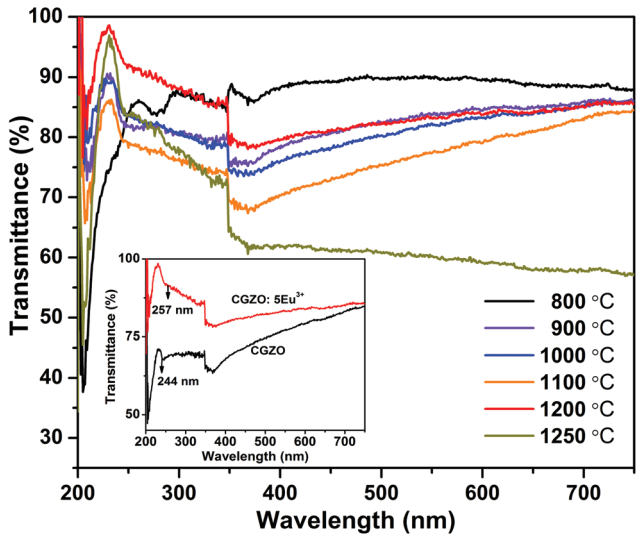

Fig. 2 Transmittance spectra of the CGZO:5Eu^{3+} phosphors obtained at different annealing temperatures (inset shows the transmittance comparison between CGZO host lattice and CGZO:5Eu^{3+} phosphor).

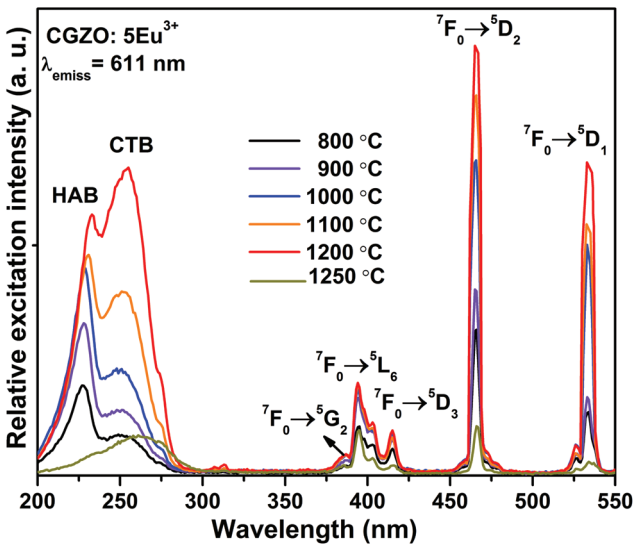

Fig. 3 PLE spectra of the CGZO:5Eu^{3+} phosphors obtained at different annealing temperatures.

are shown in the inset of Fig. 2. Furthermore, when the annealing temperature increased to 1250 °C, the transmittance decreased again due to the phase transformation with a dominant monoclinic phase of Gd^{3+} ions in the CGZO host lattice.

Fig. 3 and 4 show the PLE spectra of the CGZO:Eu^{3+} phosphors as a function of annealing temperature and Eu^{3+} ion concentration, respectively, obtained using 611 nm emission wavelength. It is noticeable that the spectral band positions in the lower energy region are similar for both annealing temperature and Eu^{3+} ion concentration variations. The PLE spectra consist of broad excitation bands such as host absorption band (HAB) and charge transfer band (CTB) with band maxima at 229 and 254 nm, respectively. Generally, the location of these band maxima depends upon the nature of the host lattice. However, in the present work, HAB and CTB positions are in good agreement with the transmittance spectra. The HAB is due to the valence to conduction band excitation,[22] and the CTB is produced by the charge transfer between the fully filled 2p orbital of O^{2-} ions and the incompletely filled 4f orbital of Eu^{3+} ions.[14] The CTB is overlapped with the f–f transitions of Gd^{3+} ions in the higher energy region, which shows very weak intensity at 275 nm ($^8S_{7/2}\rightarrow{}^6I_{11/2}$), 278 nm ($^8S_{7/2}\rightarrow{}^6I_{9/2}$), and 313 nm ($^8S_{7/2}\rightarrow{}^6P_{7/2}$) due to the efficient energy transfer from Gd^{3+} to Eu^{3+} ions. The PLE spectra of CGZO:Eu^{3+} are also composed of narrow excitation bands in the longer wavelength region due to the f–f transitions of Eu^{3+} ions. The narrow excitation peaks of the

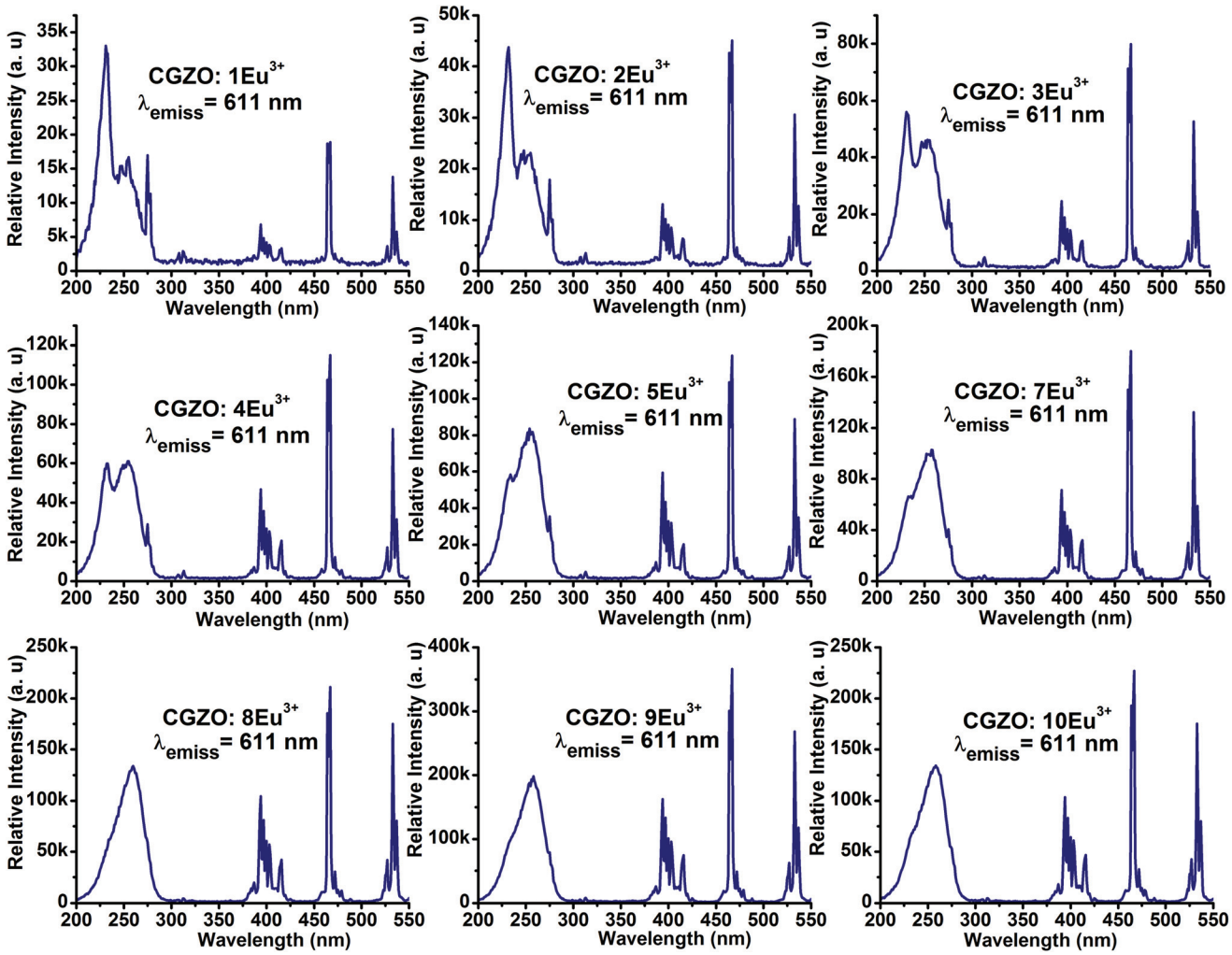

Fig. 4 PLE spectra of the CGZO:Eu^{3+} phosphors at different Eu^{3+} ion concentrations.

intra-configurational f–f transitions of Eu^{3+} ions are assigned to the electronic transitions of ($^7F_0 \rightarrow {}^5G_2$) at 385 nm, ($^7F_0 \rightarrow {}^5L_6$) at 394 nm, ($^7F_0 \rightarrow {}^5D_3$) at 416 nm, ($^7F_0 \rightarrow {}^5D_2$) at 466 nm, and ($^7F_0 \rightarrow {}^5D_1$) at 533 nm. In the PLE spectra, the ($^7F_0 \rightarrow {}^5D_2$) transition is more intense than the CTB, which is in contrast to the commercial Y_2O_3:Eu^{3+} phosphor. The main excitation peaks suggest that the CGZO:Eu^{3+} phosphors are able to generate red emission by exciting with ultraviolet (UV), near-UV (NUV) and blue laser diode/LED pumping sources.

From the variation of excitation intensities as a function of annealing temperature in Fig. 3, it was observed that the intensities of HAB at 229 nm, ($^7F_0 \rightarrow {}^5L_6$) at 394 nm, and ($^7F_0 \rightarrow {}^5D_2$) at 466 nm were much stronger as compared to the CTB when the sample is annealed at 800 °C. While on increasing the annealing temperature from 900 °C to 1200 °C, the strength of the CTB increased and the intensity of HAB decreased due to the improved energy transfer probability from the fully filled 2p orbital of O^{2-} ions and the incompletely filled 4f orbital of the Eu^{3+} ions. The reason is because the crystallite size of the particles increases and the distance between the O^{2-} and Eu^{3+} ions decreases with increasing the annealing temperature. However, the ($^7F_0 \rightarrow {}^5L_6$) and ($^7F_0 \rightarrow {}^5D_2$) transitions in the longer wavelength region increased continuously with increasing the annealing temperature. It is clear that the CTB intensity increases gradually and totally dominates the HAB after annealing at 1200 °C. The CTB maxima shifted towards the lower energy side, which facilitates the energy transfer from lowest strong absorption band to the hypersensitive transitions of Eu^{3+} ions.[23] This effect is related to an appearance of Eu^{3+}–Eu^{3+} pairs in the system because of the decrease in the average distance between the Eu^{3+} ions. This result is also consistent with the transmittance studies, where the transmittance increases suddenly at 1200 °C. Moreover, on increasing the Eu^{3+} ion concentration, the HAB and f–f transitions of Gd^{3+} ions were decreased gradually and almost disappeared at higher Eu^{3+} ion concentrations, as shown in Fig. 4. Also, the intensities of ($^7F_0 \rightarrow {}^5L_6$) and ($^7F_0 \rightarrow {}^5D_2$) transitions in the longer wavelength region and the intensity of the CTB increased with increasing the Eu^{3+} ion concentration. Particularly, the continuous enhancement in the intensity of the ($^7F_0 \rightarrow {}^5D_2$) transition in the blue region is a good sign for obtaining natural white light when mixing with YAG:Ce^{3+} yellow phosphors.

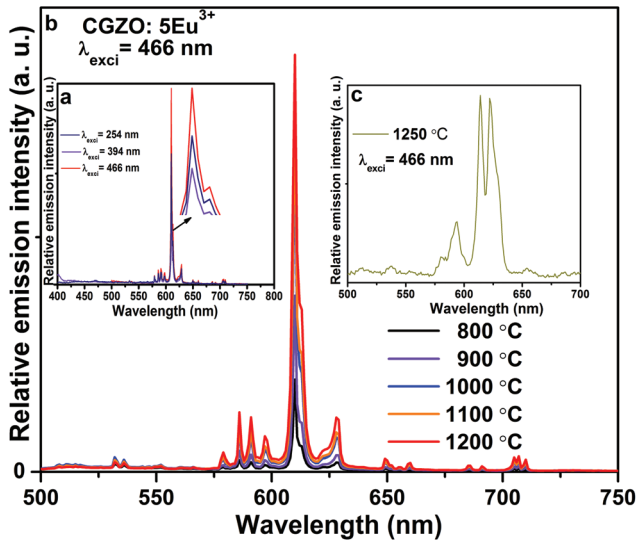

Fig. 5 PL spectra of the CGZO:5Eu^{3+} phosphors (a) after annealing at 1200 °C at different excitation wavelengths, (b) at different annealing temperatures, and (c) after annealing at 1250 °C.

Red light emission of CGZO:Eu^{3+} phosphors was so strong as to be visible to the naked eye when exciting with UV, NUV or blue wavelengths. The PL spectra of the CGZO:Eu^{3+} phosphors as a function of excitation wavelength are shown in Fig. 5(a). Evidently, these phosphors can be excited with the intense f–f transition at 466 nm ($^7F_0 \rightarrow {}^5D_2$), 394 nm ($^7F_0 \rightarrow {}^5L_6$) and CTB. As can be seen in Fig. 5(a), it is evident that the CGZO:Eu^{3+} phosphors can strongly absorb blue light and transfer the excitation energy to the red ($^5D_0 \rightarrow {}^7F_2$) transition, suggesting that the CGZO:Eu^{3+} phosphors are suitable to be excited by a blue LED chip.

Fig. 5(b) shows the PL spectra of the CGZO:Eu^{3+} phosphors as a function of annealing temperature. The spectra exhibited intense emission bands with a peak maximum at 611 nm. This can be ascribed to the forced electric-dipole also called the hypersensitive ($^5D_0 \rightarrow {}^7F_2$) transition of Eu^{3+} ions, which is located at the sites without inversion symmetry. The emission bands at 586, 591, and 598 nm with smaller intensities are due to the magnetic-dipole ($^5D_0 \rightarrow {}^7F_1$) transition of Eu^{3+} ions. The other weak emission bands of Eu^{3+} ions at 579, 650 and 705 nm are due to the ($^5D_0 \rightarrow {}^7F_0$), ($^5D_0 \rightarrow {}^7F_3$), and ($^5D_0 \rightarrow {}^7F_4$) transitions, respectively. Furthermore, it is well known that the ^7F_J energy levels of Eu^{3+} ions split into several components under the crystal-field effect.[24] C_{2v} is the highest orthorhombic symmetry that allows the full splitting of $^7F_1$ levels of Eu^{3+} ions and shows three well-resolved components, due to the completely lifted "2J + 1" degeneracy. The full splitting of the $^7F_1$ level confirmed the Eu^{3+} emission coming from the orthorhombic symmetry.

When the annealing temperature increased from 800 to 1200 °C, the intensity of the ($^5D_0 \rightarrow {}^7F_2$) transition increased significantly. The intensity ratio of ($^5D_0 \rightarrow {}^7F_2$) to ($^5D_0 \rightarrow {}^7F_1$), also called the asymmetric ratio (R), is close to being related to the local environment of Eu^{3+} ions. Usually, the larger the intensity ratio of ($^5D_0 \rightarrow {}^7F_2$) to ($^5D_0 \rightarrow {}^7F_1$), the lower the local symmetry. The asymmetric ratios of CGZO:Eu^{3+} phosphors obtained with various annealing temperatures were also calculated, and the results are shown in Table 1. The results show that the asymmetric ratio increases slightly with increasing the annealing temperature up to 1200 °C due to the increase of crystallite size, which confirms the decrease in the local symmetry and hence an increase in the red emission ($^5D_0 \rightarrow {}^7F_2$). When the annealing temperature was increased above 1200 °C, the position of the ($^5D_0 \rightarrow {}^7F_2$) transition shifted towards the longer wavelength side and the asymmetry ratio decreased due to the dominant monoclinic phase of Gd_2O_3, as shown in Fig. 5(c). From the above results, the optimized annealing temperature was 1200 °C. So, we measured the PLE and PL spectra with different concentrations at 1200 °C.

Table 1 Asymmetry ratios and CIE chromaticity coordinates after annealing at different temperatures

Annealing temperature (°C)	Asymmetry ratio (R)	CIE chromaticity coordinates
800	7.49	(0.620, 0.379)
900	8.13	(0.633, 0.367)
1000	8.47	(0.641, 0.358)
1100	8.90	(0.644, 0.356)
1200	9.07	(0.645, 0.323)

The shape and peak positions of PL emission spectra of CGZO:Eu^{3+} as a function of Eu^{3+} ion concentration upon annealing at 1200 °C were similar, as shown in Fig. 6. However, in addition to the $^5D_0$ emissions, the $^5D_{1,2}$ emissions of the higher energy levels at shorter wavelengths of 400–550 nm were observed at lower Eu^{3+} ion concentrations and gradually disappear with increasing the Eu^{3+} ion concentration due to the cross-relaxation effect. The presence of higher energy level emissions is not only dependent on the concentration, but also depends upon the phonon energies. The possible cross-relaxation channels in the CGZO host lattice are as follows:[25,26]

$$^5D_1 + {}^7F_0 \rightarrow {}^5D_0 + {}^7F_3 \text{ for depopulating the } {}^5D_1 \text{ level}$$

$$^5D_2 + {}^7F_1 \rightarrow {}^5D_1 + {}^7F_4 \text{ for depopulating the } {}^5D_2 \text{ level}$$

$$^5D_3 + {}^7F_0 \rightarrow {}^5D_2 + {}^7F_6 \text{ for depopulating the } {}^5D_3 \text{ level}$$

When the Eu^{3+} ion concentration increased from 1 to 9 mol% in the CGZO host lattice, the emission intensity also increased. As the Eu^{3+} ion concentration further increased above 9 mol%, the emission intensity decreased due to the concentration quenching. Therefore, the concentration quenching of Eu^{3+} ions in the CGZO host lattice was found to be 9 mol%. The concentration quenching has two types of origins: (i) when increasing the Eu^{3+} ion concentration in the CGZO host lattice, the excitation migration due to the resonance between the Eu^{3+} ions is increased, and thus the excitation energy reaches quenching centers, and (ii) the Eu^{3+} ions are paired or coagulated in the CGZO host lattice and are changed to quenching centers. To estimate the luminescence lifetime of the optimized CGZO:9Eu^{3+} phosphor, the decay curve was

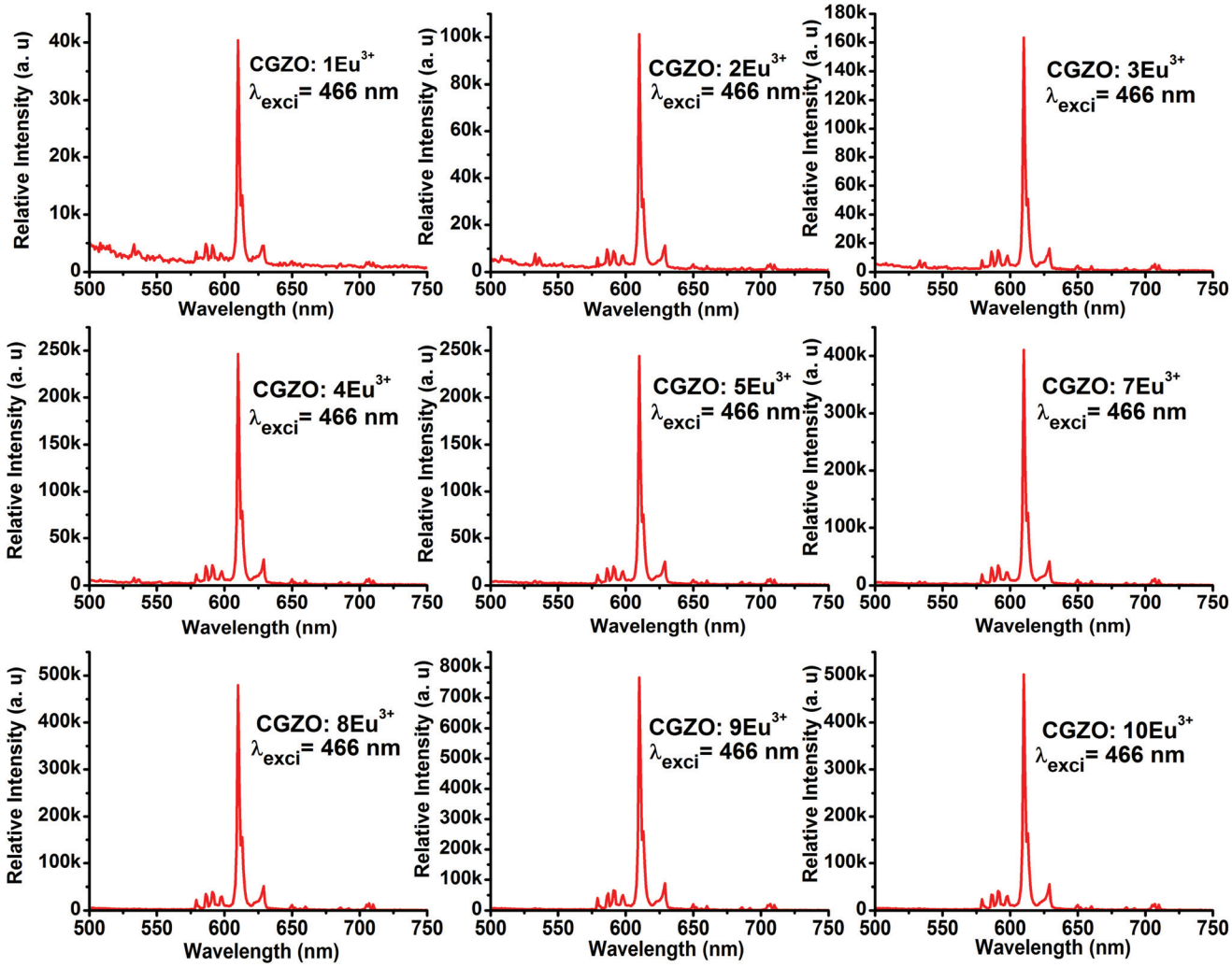

Fig. 6 PL spectra of the CGZO:Eu^{3+} phosphors at different Eu^{3+} ion concentrations.

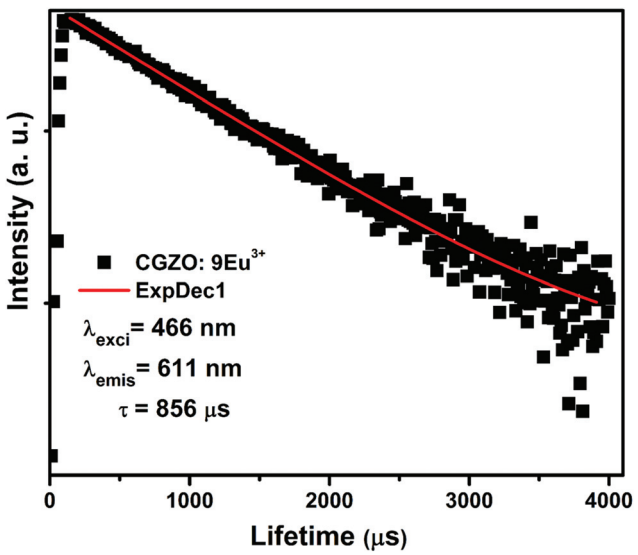

Fig. 7 Decay curve for the optimized CGZO:9Eu^{3+} phosphor.

measured under 466 nm excitation and 611 nm emission wavelengths, as shown in Fig. 7. The decay curve was well fitted to a single exponential function of $I(t) = I_0(t)\exp(-t/\tau)$, where $I(t)$ is the decaying luminescence intensity at time t, I_0 is the initial intensity and τ is the decay time. The calculated lifetime was found to be around 856 μs.

To clarify the red emission richness, the CGZO:Eu^{3+} phosphors were compared with the commercial Y_2O_3:Eu^{3+} (4.4 wt%) phosphor by monitoring the 611 nm emission wavelength, different excitation wavelengths and different concentrations of Eu^{3+} ions in the CGZO host lattice, as shown in Fig. 8(a–c). In Fig. 8(a), the blue excitation due to the ($^7F_0 \rightarrow {}^5D_2$) transition is more prominent than the CTB in the CGZO:Eu^{3+} phosphor. This is in contrast to the commercial Y_2O_3:Eu^{3+}, where the CTB dominates the excitation spectrum. Also, the blue excitation band of the CGZO:Eu^{3+} phosphor is somewhat wider than that of the commercial phosphor (inset of Fig. 8(a)), which reduces the emission wavelength control of LEDs due to the increased absorption cross-section of the phosphor.[11]

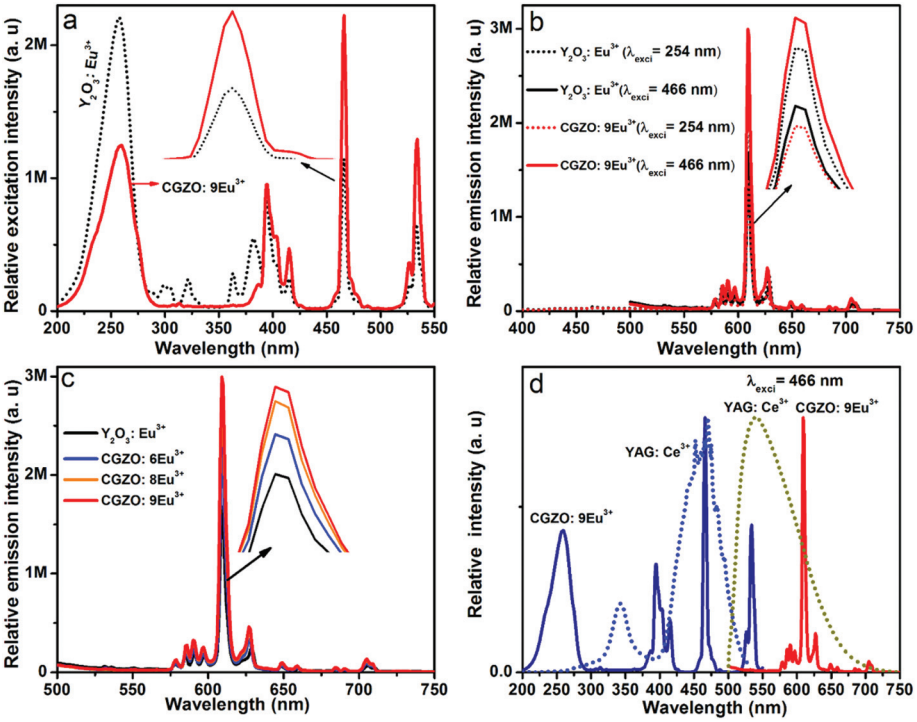

Fig. 8 (a) Comparison of PLE spectra between the CGZO:$9Eu^{3+}$ and commercial Y_2O_3:Eu^{3+} phosphors. (b) PL spectra of the CGZO:$9Eu^{3+}$ and commercial Y_2O_3:Eu^{3+} phosphors at different excitation wavelengths. (c) PL spectra of the CGZO:Eu^{3+} and commercial Y_2O_3:Eu^{3+} phosphors at different Eu^{3+} ion concentrations. (d) Identical verification of PLE and PL spectra of the CGZO:$9Eu^{3+}$ and YAG:Ce^{3+} phosphors.

Fig. 8(b) and (c) show the comparison of PL spectra at different Eu^{3+} concentrations and different excitation wavelengths. Under 466 nm excitation, the emission intensities of 6, 8 and 9 mol% Eu^{3+} ion-doped CGZO were much greater than that of the commercial Y_2O_3:Eu^{3+} phosphors. However, this is in contrast to the situation under 256 nm excitation. It is also noted that the most intense transition is at 611 nm, which is the best red component for high luminous efficacy WLEDs, and the weak emission due to the ($^5D_0 \rightarrow {}^7F_4$) transition in the deep red region indicates the higher luminous efficacy of radiation.[11] The *R* value for the Y_2O_3:Eu^{3+} is 8.75; however, for CGZO:$6Eu^{3+}$, CGZO:$8Eu^{3+}$, and CGZO:$9Eu^{3+}$, it is 9.20, 9.35, and 9.46, respectively. The increased *R* value indicates the improved color purity of the red component of the CGZO:Eu^{3+} phosphors. Furthermore, the CGZO:$9Eu^{3+}$ phosphor can also assist as a red compensator in the fabrication of $Y_3Al_5O_{12}$ (YAG):Ce^{3+} yellow phosphor-based WLEDs for indoor illumination. With an appropriate amount of CGZO:$9Eu^{3+}$ phosphor combined with YAG:Ce^{3+}, as shown in Fig. 8(d), an excellent white-light emission might be possible because the excitation peaks of the CGZO:Eu^{3+} at 466 and 533 nm were overlapped well with the respective excitation and emission peaks of the YAG:Ce^{3+} phosphor. Hence, it is assumed that when the YAG:Ce^{3+} phosphor is excited at 466 nm, the excitation and/or emission spectra of YAG:Ce^{3+} may serve as an excitation source to the CGZO:Eu^{3+}, thus leading to a yellow emission including red emission being obtained. This kind of pc-WLED can contribute to high CRI display systems and pleasant atmosphere for indoor illumination.

Based on the integrating sphere method, the absolute quantum yield (η) of CGZO:$9Eu^{3+}$ nanophosphor as a function of excitation wavelength was measured. For the current synthesis condition, the η values were 36, 6, 20 and 24% at the excitation wavelengths of 254, 394, 466, and 533 nm, respectively. As compared to 466 nm excitation, 533 nm excitation shows higher η. This enhanced η might be due to the absence of higher energy level emissions of Eu^{3+} ions under 533 nm excitation. It is also noticeable that the η value of commercial Y_2O_3:Eu^{3+} under 466 nm excitation is <1%,[21] which is much less than that of CGZO:$9Eu^{3+}$ nanophosphor. Mishra *et al.* reported a value of 23% for CGZO:$15Eu^{3+}$ nanophosphor,[21] which is a little higher than that of CGZO:$9Eu^{3+}$ phosphor due to the higher Eu^{3+} ion concentration and higher annealing temperature.

To explore the potentiality of the CGZO:Eu^{3+} phosphor for efficient red region emission in FED systems, the CL properties of CGZO:Eu^{3+} phosphors as a function of accelerating voltage and filament current were investigated. Fig. 9(a) shows the comparison between the CL spectra of Y_2O_3:Eu^{3+} and CGZO:$9Eu^{3+}$ phosphors under low electron beam excitation at 5 kV of accelerating voltage and 55 μA of filament current. It is observed that there is a small difference between the CL and PL spectra. At higher Eu^{3+} ion concentrations, only the $^5D_0$ emissions were observed in the PL spectrum and almost all the emissions in the higher energy regions disappeared. However, in the CL spectra, low-intensity emission bands appeared from $^5D_1$ and $^5D_2$ higher energy levels. This can be

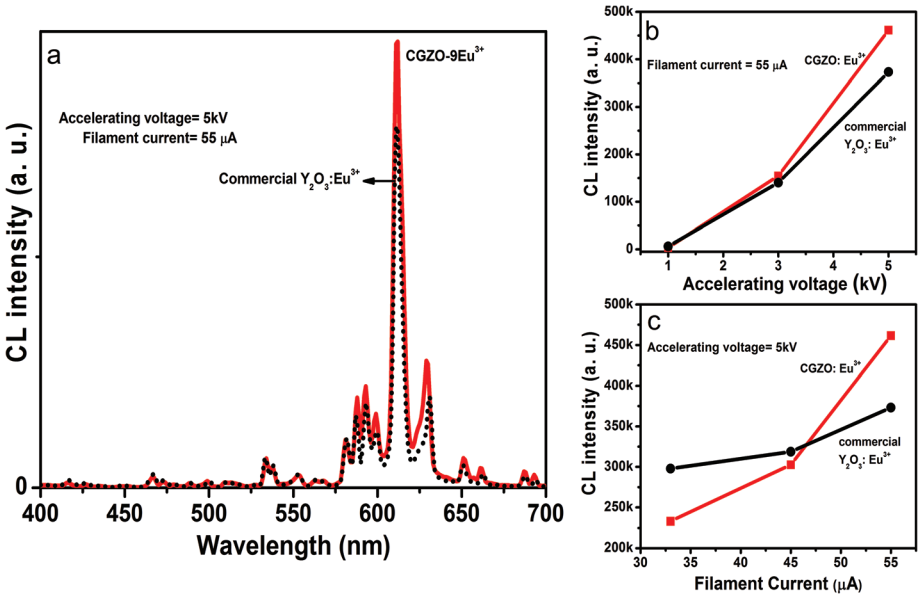

Fig. 9 (a) Comparison of CL spectra between the CGZO:9Eu^{3+} and commercial Y_2O_3:Eu^{3+} phosphors, and CL spectra of the CGZO:9Eu^{3+} and commercial Y_2O_3:Eu^{3+} phosphors as a function of (b) accelerating voltage and (c) filament current.

explained by the fact that there is a different mechanism between CL and PL. In CL, the high-energy electrons with the acceleration of anode voltage can be regulated from few electron volts to thousands of electron volts.[27,28] Therefore, the Eu^{3+} ions in the host material are excited with much higher energy as compared to the photon-based PL. Furthermore, the CL spectrum of CGZO:9Eu^{3+} shows a better emission intensity than that of commercial Y_2O_3:Eu^{3+}.

Fig. 9(b) and 9(c) show the CL intensities of the CGZO:Eu^{3+} and commercial Y_2O_3:Eu^{3+} phosphors as a function of accelerating voltage and filament current. When the accelerating voltage increased from 1 to 5 kV at a fixed filament current of 55 μA, the CL intensity of both phosphors increased and no optimization was observed up to 5 kV. A similar increment was observed for both samples on increasing the filament current from 35 to 55 μA under a fixed accelerating voltage of 5 kV as shown in Fig. 9(c). The reason is that more plasma will be produced when increasing the filament current or accelerating voltage due to the greater electron penetration depth by the recombination of more electron–hole (exciton) pairs, resulting in more Eu^{3+} ions from the boundary or surface including the inside of particles being excited.[29] The increased CL intensity with increasing accelerating voltage and filament current indicates the possibility of promising applications in the development of FED systems.

The Commission Internationale de l'Eclairage (CIE) chromaticity coordinates of the CGZO:Eu^{3+} and commercial Y_2O_3:Eu^{3+} phosphors were investigated as a function of excitation wavelength. Under 254 nm excitation, the CIE coordinates of Y_2O_3:Eu^{3+} phosphors were (0.650, 0.346), while, under 466 nm excitation, the CIE coordinates of CGZO:Eu^{3+} phosphors were (0.657, 0.341), as shown in Fig. 10. Clearly, the CGZO:Eu^{3+} phosphor has a higher red color purity under

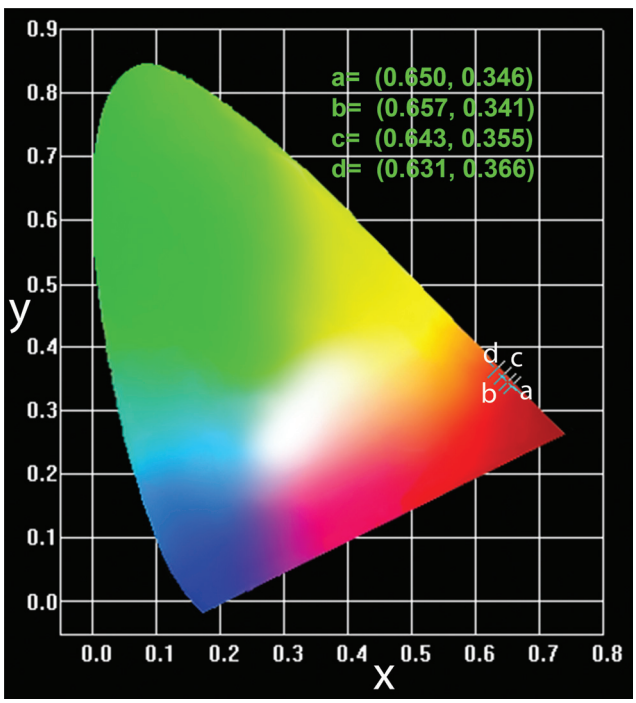

Fig. 10 CIE chromaticity coordinates from PL of (a) CGZO:9Eu^{3+} (under 466 nm excitation) and (b) commercial Y_2O_3:Eu^{3+} (under 254 nm excitation), and from CL of (c) CGZO:9Eu^{3+} and (d) commercial Y_2O_3:Eu^{3+} phosphors at an accelerating voltage of 3 kV and filament current of 55 μA.

466 nm excitation as compared to that of Y_2O_3:Eu^{3+} phosphors at 254 nm excitation wavelength. The CIE coordinates at different annealing temperatures are presented in Table 1. Also, both CGZO:Eu^{3+} and commercial Y_2O_3:Eu^{3+} phosphors show similar behavior of CIE coordinates under the low

Table 2 CIE chromaticity coordinates of CGZO:9Eu^{3+} and Y_2O_3:Eu^{3+} as a function of accelerating voltage and filament current

CIE chromaticity coordinates		
Function	CGZO:9Eu^{3+}	Commercial Y_2O_3:Eu^{3+}
Accelerating voltage (kV)		
1	(0.600, 0.392)	(0.601, 0.386)
3	(0.643, 0.355)	(0.631, 0.366)
5	(0.629, 0.368)	(0.621, 0.375)
Filament current (μA)		
33	(0.641, 0.357)	(0.629, 0.368)
45	(0.639, 0.359)	(0.621, 0.375)
55	(0.629, 0.368)	(0.621, 0.375)

beam electron excitation, and the calculated CIE coordinates related to CL spectra are summarized in Table 2. The optimized coordinates are presented in the CIE diagram in Fig. 10. From the CL-related CIE coordinates, it is understood that the color purity of red emission decreases with increasing the accelerating voltage and filament current due to the presence of higher ^5D_J levels of Eu^{3+} ions. The appearance of higher ^5D_J levels is due to the greater penetration depth, as explained above. The CIE coordinates of CL spectra indicate the red color purity of Eu^{3+} ions not only depends upon the asymmetric ratio but also relies upon the presence of higher energy $^5D_{J(=3,2,1)}$ emission levels. From the CIE chromaticity of both PL and CL spectra, CGZO:Eu^{3+} shows better emission than that of the commercial Y_2O_3:Eu^{3+} in the red region, which is useful for fabricating artificial white light to be similar to that of natural white light because of the better spectral overlap.[30,31]

Conclusion

The annealing temperature and Eu^{3+} ion concentration effects on the structural and luminescent properties of orthorhombic phase CGZO:Eu^{3+} phosphors prepared by the sol–gel process were systematically investigated. The transmittance and phase changes of CGZO:Eu^{3+} phosphors correlated with each other. The PLE spectra of these phosphors exhibited a dominant blue excitation in the visible region and the intensity increased significantly with increasing the annealing temperature and Eu^{3+} ion concentration. This performance is appropriate for obtaining natural white light emission when mixing with YAG:Ce^{3+} yellow phosphor. Detailed analytical data revealed that the PL intensity of CGZO:Eu^{3+} under 466 nm excitation dominates the commercially available Y_2O_3:Eu^{3+} phosphor under 254 nm excitation at similar measurement conditions. Concentration quenching of Eu^{3+} emission from the CGZO host lattice was observed when the Eu^{3+} doping level exceeded 9 mol%. Furthermore, the CL spectra also exhibited similar behavior to the PL spectra and the CGZO:Eu^{3+} dominated the commercial Y_2O_3:Eu^{3+} phosphor emission. From the observed luminescent properties, we are able to conclude that CGZO:Eu^{3+} under excitation of 466 nm blue wavelength is a promising red phosphor for applications in LEDs with natural white emission and high CRI optical display systems.

Acknowledgements

This work was supported by a grant from the Kyung Hee University in 2013 (KHU-20131563), and also supported by the National Research Foundation of Korea (NRF) grant funded by the Korea government (MSIP) (no. 2013-068407).

References

1 R. Lv, G. Yang, Y. Dai, S. Gai, F. He and P. Yang, *CrystEngComm*, 2014, **16**, 9612–9621.
2 G. Seeta Rama Raju, E. Pavitra, G. Purnachandra Nagaraju, K. Ramesh, B. F. El-Rayes and J. S. Yu, *Dalton Trans.*, 2014, **43**, 3330–3338.
3 G. Seeta Rama Raju, E. Pavitra, G. P. Nagaraju, R. Kandimalla, B. F. El-Rayes and J. S. Yu, *Cryst. Growth Des.*, 2013, **13**, 4051–4058.
4 C.-H. Kim, I.-E. Kwon, C.-H. Park, Y.-J. Hwang, H.-S. Bae, B.-Y. Yu, C.-H. Pyun and G.-Y. Hong, *J. Alloys Compd.*, 2000, **311**, 33–39.
5 J. T. Ingle, R. P. Sonekar, S. K. Omanwar, Y. Wang and L. Zhao, *Opt. Mater.*, 2014, **36**, 1299–1304.
6 P. Pust, V. Weiler, C. Hecht, A. Tücks, A. S. Wochnik, A.-K. Henß, D. Wiechert, C. Scheu, P. J. Schmidt and W. Schnick, *Nat. Mater.*, 2014, **13**, 891–896.
7 D. Hou, X. Xu, M. Xie and H. Liang, *J. Lumin.*, 2014, **146**, 18–21.
8 R. Dey, A. Pandey and V. K. Rai, *Spectrochim. Acta, Part A*, 2014, **128**, 508–513.
9 R. Dey and V. K. Rai, *Dalton Trans.*, 2014, **43**, 111–118.
10 N. Kaneko, M. Hagiwara and S. Fujihara, *ECS J. Solid State Sci. Technol.*, 2014, **3**, R109–R114.
11 M. Nyman, M. A. Rodriguez, L. E. Shea-Rohwer, J. E. Martin and P. P. Provencio, *J. Am. Chem. Soc.*, 2009, **131**, 11652–11653.
12 C. C. Lin and R.-S. Liu, *J. Phys. Chem. Lett.*, 2011, **2**, 1268–1277.
13 G. Li and J. Lin, *Chem. Soc. Rev.*, 2014, **43**, 7099–7131.
14 G. S. R. Raju, Y. H. Ko, E. Pavitra, J. S. Yu, J. Y. Park, H. C. Jung and B. K. Moon, *Cryst. Growth Des.*, 2012, **12**, 960–969.
15 L. Krishna Bharat, J. Y. Park and J. S. Yu, *Chem. Eng. J.*, 2014, **240**, 179–186.
16 G.-H. Lee and S. Kang, *J. Lumin.*, 2011, **131**, 2606–2611.
17 E. Pavitra, G. S. R. Raju and J. S. Yu, *Phys. Status Solidi RRL*, 2013, **7**, 224–227.
18 Sheetal, V. B. Taxak, S. Singh, Mandeep and S. P. Khatkar, *Optik*, 2014, **125**, 6340–6343.
19 I. Etchart, A. Huignard, M. Berard, M. N. Nordin, I. Hernandez, R. J. Curry, W. P. Gillin and A. K. Cheetham, *J. Mater. Chem.*, 2010, **20**, 3989–3994.

20 D. Xu, D. Haranath, H. He, S. Mishra, I. Bharti, D. Yadav, B. Sivaiah, B. Gahtori, N. Vijayan, A. Dhar, J. Zhu, V. Shanker and R. Pandey, *CrystEngComm*, 2014, **16**, 1652–1658.
21 S. Mishra, R. Rajeswari, N. Vijayan, V. Shanker, M. K. Dalai, C. K. Jayasankar, S. Surendra Babu and D. Haranath, *J. Mater. Chem. C*, 2013, **1**, 5849–5855.
22 A. Lakshmanan, *Luminescence and Display Phosphors: Phenomena and Applications*, Nova Science Publishers, 2008.
23 G. Blasse and B. Grabmaier, *Luminescent materials*, Springer, 1994.
24 X. Y. Chen and G. K. Liu, *J. Solid State Chem.*, 2005, **178**, 419–428.
25 Z. Hao, J. Zhang, X. Zhang and X. Wang, *Opt. Mater.*, 2011, **33**, 355–358.
26 D. Hreniak, W. Stręk, P. Dereń, A. Bednarkiewicz and A. Łukowiak, *J. Alloys Compd.*, 2006, **408–412**, 828–830.
27 G. Seeta Rama Raju, E. Pavitra and J. S. Yu, *Phys. Chem. Chem. Phys.*, 2014, **16**, 18124–18140.
28 X.-J. Wang, R.-J. Xie, B. Dierre, T. Takeda, T. Suehiro, N. Hirosaki, T. Sekiguchi, H. Li and Z. Sun, *Dalton Trans.*, 2014, **43**, 6120–6127.
29 G. Li, Z. Hou, C. Peng, W. Wang, Z. Cheng, C. Li, H. Lian and J. Lin, *Adv. Funct. Mater.*, 2010, **20**, 3446–3456.
30 L. S. Kumari, P. P. Rao, M. Thomas and P. Koshy, *J. Electrochem. Soc.*, 2009, **156**, P127–P131.
31 S. Fujihara and K. Tokumo, *Chem. Mater.*, 2005, **17**, 5587–5593.